Thin-film composite membranes with nanocomposite substrate modified with graphene oxide/TiO$_2$ for forward osmosis process

Fang Li[a,b,*], Feng Zhao[a], Manhong Huang[a], Chunyan Ma[a,*], Bo Yang[a], Qing Tian[a,b]

[a]*School of Environmental Science and Engineering, Donghua University, Shanghai 201620, China, Tel. +86-21-67792544;*
Fax: +86-21-62373312; email: lifang@dhu.edu.cn (F. Li), Tel. +86-21-67792557; Fax: +86-21-6779253; emails: machunyan@dhu.edu.cn (C. Ma),
747220120@qq.com (F. Zhao), 1003154817@qq.com (M. Huang), yangbo@dhu.edu.cn (B. Yang), tq2004@dhu.edu.cn (Q. Tian)
[b]*Textile Pollution Controlling Engineering Center of Ministry of Environmental Protection, Shanghai 201620, China*

ABSTRACT

Thin-film composite (TFC) membranes incorporating nanofillers of TiO$_2$ and graphene oxide (GO) in polyethersulfone (PES) substrates were fabricated for forward osmosis (FO) process in the present work. The modified PES substrates by phase inversion and FO membranes by interfacial polymerization were characterized by scanning electron microscopy, atomic force microscopy and contact angle. The synergistic effect of the nanofillers on the transport properties and antifouling performance of the TFC membranes with nanocomposite substrate (NS) was investigated by fouling test. The result showed that the substrates incorporating nanofillers exhibited improved hydrophilicity, greater porosity and higher water flux than the neat samples. Addition of the nanofillers in PES substrates remarkably improved the water permeance of TFC membranes with the drawback of the increase of reverse salt flux. Comparing to single filler, the combination of GO and TiO$_2$ as fillers in the substrate was proved to effectively enhance the antifouling ability of the TFC-NS membranes.

Keywords: Graphene oxide; Forward osmosis; TiO$_2$; Fouling; Synergistic effect

1. Introduction

Membrane separation process is one of the most important techniques to solve the scarcity of freshwater [1]. In current, high quality water can be obtained by traditional pressure-driven membrane processes, including microfiltration, ultrafiltration, nanofiltration or reverse osmosis. Although these membrane processes have high separation efficiency, the application in water and wastewater treatment is limited for the shortcomings, like membrane fouling, high energy cost and chemical washing. Recently, forward osmosis (FO) process has received increasing attention defining FO as "low energy process" for it is driven by the difference of osmotic pressure between a draw solution (DS) and a feed solution (FS) through a semi-permeable membrane. However, internal concentration polarization (ICP)

is a dominant factor resulting in low water flux in FO process which is caused by a net osmotic pressure difference across the membrane, as the actual net osmotic pressure is remarkably less than the theoretical osmotic pressure [2]. Hence, an ideal support layer for a FO membrane should be highly porous, low tortuous and thin in structure [3].

The incorporation of nanomaterials as fillers into polymer matrix has attracted great attention in the membrane fabrication [4]. A various nanomaterials, such as TiO$_2$ [5], graphene oxide (GO) [6] and Al$_2$O$_3$ [7], were used widely to improve the performance of membranes due to their high chemical stability, super hydrophilicity, acceptable photochemical reactivity and potential of antifouling ability. A large number of research reports had proved that the nanofillers exerted significant effect on membrane structure. It was observed that an appropriate loading of nanofiller in polymer matrix resulted in the increased porosity and mean pore size. Chang et al. [8] prepared asymmetric polyvinylidene fluoride (PVDF) composite ultrafiltration

* Corresponding author.

membranes containing GO by using *N*-methylpyrrolidone as solvent and polyvinylpyrrolidone (PVP) as the pore forming reagent and found that the surface hydrophilicity and anti-fouling performance were enhanced by the synergistic effects of incorporated GO and PVP. Wang et al. [9] used reduced GO modified graphitic carbon nitride (g-C$_3$N$_4$) as a modifier for porous polyethersulfone (PES) substrate for the preparation of thin-film composite membranes with nanocomposite substrate (TFC-NS) membranes. The result showed that the FO performance improvement should be attributed to the modified structure of the PES substrate, and thus lower structure parameter and the reduction of ICP. However, excess nanofiller content led to adverse effect on the membrane performance as the high density fillers caused to the agglomeration of nanoparticles. Consequently, the aggregated clusters blocked and collapsed the membrane pores, deteriorated the membrane permeability. Ionita et al. [10] found that the flux of the PS/GO loose composite membranes by phase-inversion method decrease with GO addition and it was assigned to the stabilization of composite membrane structure. Thus, the dispersion of the nanofiller in the polymer matrix played an important role during the fabrication of TFC-NS membranes.

Both GO and TiO$_2$ have been generally acknowledged as the promising nanofillers to improve the performance of membrane. Although a lot of work on the incorporation of nanoparticles into the membrane matrix to enhance the membrane performance had been carried out, the synergistic effect of two blending nanoparticles has seldom been studied. In this work, the nanocomposite PES substrate by incorporating GO and TiO$_2$ in the PES matrix was prepared. The TFC membranes with TFC-NS membranes for FO process were synthesized by interfacial polymerization. The combination of TiO$_2$ and GO nanoparticles was expected to mitigate the positive nanoparticle agglomeration with low individual nanoparticle loading. The synergistic effect of TiO$_2$ and GO as nanofiller could improve the structure of FO membrane support layer and enhance the antifouling ability. The antifouling property of the TFC-NS membranes incorporated nanofillers was studied through the evaluation of flux decline in a filtration of model foulant solution.

2. Materials and methods

2.1. Chemicals and reagents

PES (E3010), supplied by BASF (Guangzhou, China), was used as the polymer material to prepare the substrate as the support layer of TFC FO membranes. *N,N*-Dimethylacetamide (DMAc, 99.8%), PVP (K30), 1,3-phenylenediamine (MPD, >99%), trimesoyl chloride (TMC, >99%), sodium chloride were purchased from Sigma-Aldrich (China). Bovine serum albumin (BSA) was purchased from Aladdin Co. (Shanghai), to be used for the exploration of membrane fouling. TiO$_2$ nanoparticles (CAS: 13463-67-7) used in the present study were obtained from Aladdin Co. (Shanghai). Graphite powders were produced by the Qingdao Ruisheng Graphite Co., Ltd. (Shandong, China).

2.2. Fabrication of substrates and TFC membranes

2.2.1. Preparation of GO nanosheets

GO was prepared by improved Hummers' method, as described elsewhere [11]. In brief, a 9:1 mixture of concentrated H$_2$SO$_4$/H$_3$PO$_4$ (360:40 mL) was added to a mixture of graphite flakes (3.0 g) and KMnO$_4$ (18.0 g), producing a slight exotherm to 35°C–40°C. The reaction was then heated to 50°C and stirred for 12 h. The reaction was cooled to room temperature and poured onto ice (400 mL) with 30% H$_2$O$_2$ (3 mL). The filtrate was centrifuged (4,000 rpm for 4 h), and the remaining solid material was then washed in succession with 200 mL of water, 200 mL of 30% HCl and 200 mL of ethanol. The material remaining after this extended, multiple-wash process was coagulated with 200 mL of ether, and the resulting suspension was filtered over a 0.45 µm PVDF membrane. The solid obtained on the filter was vacuum-dried overnight at room temperature, obtaining 5.8 g of product.

2.2.2. Fabrication of PES and nanocomposite substrates

The PES support layer was prepared by non-solvent induced phase-inversion process. First, PES, PVP and GO were dissolved in DMAc solution and stirred at 70°C for 4 h, as shown in Table 1. Then, the solution set down for 1 h. A membrane casting knife (12303, Elcometer) was used to spread the casting solution onto the clean glass plate with a thickness of 150 µm. Next, the cased film was immediately immersed into a coagulant bath filled with deionized (DI) water at room temperature (20°C) to initiate the phase separation. Last, the PES support layer was remained in the water bath for 10 min before transfer to a DI water bath for storage. The composition and concentration of dope solutions and monomer solutions for the substrate and TFC membranes preparation are also summarized in Table 1.

Table 1
Composition and concentration of casting solutions and monomer solutions for the preparation of the substrates and FO membranes

Substrate	Support layer preparation					FO membrane	Active layer preparation	
	PES (wt%)	PVP (wt%)	DMAc (wt%)	GO (wt%)	TiO$_2$ (wt%)		MPD (wt%)	TMC (wt/v%)
PES	16	5	79	0	0	TFC	2	0.1
PES-T1.0			78	0	1.0	TFC-NS-T1.0		
PES-T0.5			78.5	0	0.5	TFC-NS-T0.5		
PES-T0.5/G0.5			78	0.5	0.5	TFC-NS-T0.5/G0.5		
PES-G0.5			78.5	0.5	0	TFC-NS-G0.5		
PES-G1.0			78	1.0	0	TFC-NS-G1.0		

2.2.3. Fabrication of TFC and TFC-NS membranes

The active layer (AL) of FO membranes was prepared by interfacial polymerization on the top surface of the PES substrates. The substrates were heated in 70°C DI water bath for 2 min, and then soaked in a 2 wt% MPD solution. After removing the excess MPD by an air gun, a 0.1% w/v% TMC in *n*-hexane solution was poured onto the MPD-soaked PES substrates for 1 min to form polyamide (PA) AL. After the interfacial polymerization, the membranes were placed into air blowing thermostatic oven in 60°C for 8 min. The membranes were rinsed in DI water to remove the residual regents, and then stored in DI water before using. Their preparation conditions are also summarized in Table 1.

2.3. Evaluation of the membrane performance

2.3.1. Osmotic flux testing

A laboratory scale, cross-flow reverse osmosis unit was utilized to determine the water permeance (A) and salt permeability coefficient (B), as shown in Fig. S1. The water permeance coefficient of the FO membranes, A, was acquired as Eqs. (1) and (2):

$$J = \frac{\Delta V}{A_m \Delta t} \tag{1}$$

$$A = \frac{J}{\Delta P} \tag{2}$$

where J, A, A_m, ΔV, Δt and ΔP are water flux, water permeance, the effective membrane area, the permeate volume, time and cross-membrane pressure, respectively.

DI water was used as feed during the acquisition of A. Subsequently, the salt rejection, R, was determined from the measured conductivities of permeate and feed by using feed-water containing 2,000 ppm NaCl at 5 bar with a cross-flow velocity of 0.25 m/s. The flux was recorded for 1 h to calculate the A coefficient:

$$R = \left(1 - \frac{C_p}{C_f}\right) \times 100\% \tag{3}$$

where C_p and C_f are the salt concentrations of the permeate and FS, respectively. The salt permeability coefficient, B, an intrinsic property of membrane skin layer, was calculated based on the solution-diffusion theory [12].

$$B = \left(\frac{1}{R} - 1\right) \times J \tag{4}$$

2.3.2. Membrane structural parameter

The FO membrane performance including water flux and reverse salt flux was evaluated with a laboratory scale FO setup as described in other literature [13]. As shown in Fig. S2, a cross-flow membrane filtration cell unit with an effective filtration area of 40 cm² was applied to test TFC and TFC-NS membranes, similar to previous investigations. This membrane module contained channels on both sides for FS and DS, respectively. The effective dimensions of each channel were measured as 10 cm (length), 4 cm (width) and 2.0 mm (height). The temperature of the FS and DS were maintained at 25°C ± 1°C. DI water and 1.0 M NaCl solution were used as the FS and raw solution, respectively. The experimental water flux, J_v, was calculated by measuring the change in the feed container mass with time as follows:

$$J_V = \frac{\Delta V}{A_m \times \Delta t} = \frac{\Delta m / \rho}{A_m \times \Delta t} \tag{5}$$

where A_m is the effective membrane surface area, Δt is the measuring time interval, ρ is the water density and Δm is the measured weight interval for the water that permeated from the FS to the DS. The reverse salt flux J_s of the DS was calculated as:

$$J_s = \frac{\Delta(C_t V_t)}{A_m \times \Delta t} \tag{6}$$

where C_t and V_t are the concentration and volume of FS at the end of each test, respectively. As for FO membrane, the structure parameter is one of the essential properties. In addition to this, the classical ICP model is also determining membrane structural parameter (S), as the following equation [13]:

$$J_V = \frac{D}{S}\left[\ln \frac{A\pi_{draw} - J_v + B}{A\pi_{feed} + B}\right] \tag{7}$$

$$J_V = \frac{D}{S}\left[\ln \frac{A\pi_{draw} + B}{A\pi_{feed} + J_v + B}\right] \tag{8}$$

where D is the salt diffusion coefficient, π_{draw} and π_{feed} are the osmotic pressures of the DS and FS.

2.4. Organic fouling testing

The dynamic fouling filtration was conducted with the control TFC and TFC-NS membranes in the laboratory scale FO unit using a mixture of BSA (100 mg/L) as the feed and 2 M NaCl as the DS. The protocol of the dynamic fouling filtration in our work was similar to the method described elsewhere [14]. First, a controlled experiment was conducted with an FS of DI water to measure the extent of flux decline exclusively due to DS dilution and solute reverse diffusion. Then, the fouling experiment was conducted at the same initial flux as the controlled experiment with BSA solution as feed. In this case, the flux decline observed is caused by the combined effect of DS dilution, solute reverse diffusion and membrane organic fouling. The controlled and fouling experiments were conducted up to a cumulative permeate volume of 500 mL. FD$_{500}$ was considered as a parameter to evaluate the flux decline of fouling [14].

$$FD_{500} = \frac{\left|(J_v - J_{v0})_b - (J_v - J_{v0})_f\right|}{(J_v - J_{v0})_c} \tag{9}$$

where the subscript 500 mL indicates that the normalized baseline $(J_v/J_{v0})_b$ and fouling fluxes $(J_v/J_{v0})_f$ and, respectively, are measured at 500 mL of collected permeate volume.

2.5. Membrane characterization

The morphologies of the membranes were examined by scanning electron microscopy (SEM, JSM-5600LV, Japan). The pore size of the substrate is measured by scientific analysis software, i.e., ImageJ. The atomic force microscopy (AFM) measurements were performed on a multimode AFM with Nanoscope IV Multi Mode Controller (Veeco, USA) using the software supplied by the manufacturer. The membrane surface was characterized by using the attenuated total reflectance Fourier transform infrared (ATR-FTIR) spectroscopy (Bruker, Tensor27, German). The contact angle (CA) measurements were performed using a CA goniometer (SL-200c, Shanghai Solon Technology Science Co., Ltd., Shanghai, China). The data were reported as the average values and standard deviations of six measurements. Thermogravimetric analysis was carried out on HTG-1 thermal analyzer. The sample was tested at a heating rate of 10°C/min under N_2 atmosphere with a flow rate of 10 mL/min.

For the measurement of the substrate membrane porosity ε (%), Eq. (10) was employed by taking into account the change in membrane weight before and after drying:

$$\varepsilon = (w_1 - w_2) / A_m \delta \rho \tag{10}$$

where W_1 and W_2 are the weight of wet membrane and dry membrane, respectively.

3. Results and discussion

3.1. Characterization of GO nanosheets

To confirm GO nanosheets were obtained via the improved Hummers' method, the product was characterized by FTIR, X-ray diffraction (XRD), SEM and transmission electron microscope (TEM), as shown in Fig. 1. The peaks at 3,400 and 1,400 cm^{-1} of the GO nanosheets were assigned to O–H stretching and O–H deformation, respectively [15]. The C=O stretching vibrations in the carboxyl group of GO were obviously visible around 1,725 cm^{-1}, whereas the peak at 1,075 cm^{-1} was due to the C–C stretching of epoxy and alkoxy groups. The peak at 1,627 cm^{-1} was assigned to the vibrations of the adsorbed water molecules and the contributions from the vibration of aromatic C=C [16]. As for the XRD patterns, the broad and relatively weak diffraction peak at $2\theta = 10.7°$ ($d = 0.87$ nm), which corresponds to the typical diffraction peak of GO nanosheets, is attributed to the (002) plane [17]. The SEM and TEM images of GO prepared by modified oxidation method is presented in Figs. 1(c) and (d). According to the SEM image, GO formed big smooth plates of size ~4 μm.
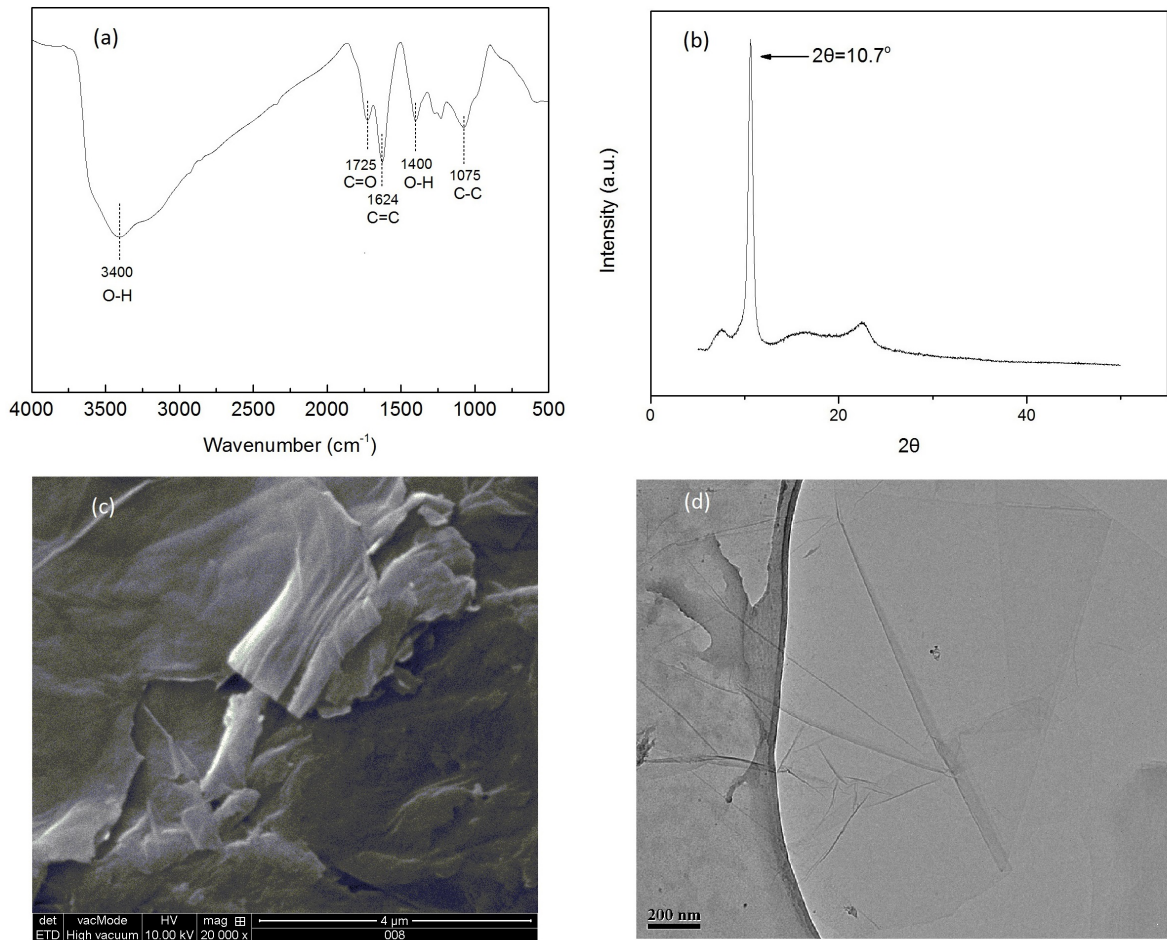

Fig. 1. Characterization of GO nanosheets via ATR-FTIR (a), powder XRD (b), SEM (c) and TEM (d).

The GO nanosheet folding can easily be observed since the GO sheets lose their flat nature and display some sort of folding morphology on their surface and at the edges when the graphite was oxidized [18,19].

3.2. Characterization of the substrates

3.2.1. Hydrophilicity and permeability

CA is an important parameter to evaluate the hydrophilicity of membranes that is relative to the flux and the antifouling ability of a membrane. Table 2 presents the difference in the properties of PES substrates with various nanofiller loadings. Obviously, the hydrophilicity of PES substrates was improved due to the high hydrophilicity of the incorporated nanofillers, i.e., GO and TiO_2. The CA of TiO_2 nanoparticles has been reported to be around 10°, which means TiO_2 nanoparticle has a very hydrophilic surface [20]. The CA of the PES substrate, about 95.7°, decreased to 73.8° when the NSs were incorporated with 0.5 wt% TiO_2 and decreased to 76.9° with 1.0 wt% TiO_2. This result was basically coincident to the founding of Razmjou et al. [21] that the addition of TiO_2 itself could increase the hydrophilicity by around 18% regardless of the amount of nanoparticles in polymer matrix. As for the GO nanosheets, the oxygen-containing groups such as carboxyl (C–O–OH), hydroxyl (C–OH), epoxide (C–O–C) covalently decorating on the flake render to the GO nanofiller high hydrophilicity. During the phase-inversion process, the hydrophilic nanofillers, i.e., TiO_2 and GO, migrate spontaneously to membrane surface when the NSs formed in water [22]. Thus, the NSs with half-embedded nanoparticles on surface exhibited more hydrophilic than the neat PES substrates.

However, it can be found from Table 2 that GO nanofillers can contribute more hydrophilicity for PES substrates than TiO_2 with the equal loading. However, the hydrophilicity of the membrane surface did not increased with the nanofiller loading. In contrast, the CA value of NSs with 1.0 wt% nanofillers was higher than that with 0.5 wt% nanofillers for both GO and TiO_2. It can be explained that CA value was influenced by surface morphology in addition to surface energy. For the NS, excessive nanofiller loading could deteriorate the hydrophilicity due to the agglomeration of nanofillers on membrane surface [23]. The agglomeration of GO might be more severe with comparison of TiO_2, as the CA increased from 58.7° to 71.7° when the GO loading of 0.5 wt% increased to 1.0 wt%. Yet, the combination of TiO_2 and GO in NS can

enhance the hydrophilicity more effectively than the sole type nanofiller, which was indicated in Table 2. The CA of the PES-T0.5/G0.5 was lower than that of PES-T1.0 and PES-T1.0 although these NSs had the equal total nanofiller loading of 1.0 wt%.

Table 2 also presents the overall porosity of the neat and NSs. It can be found that the membrane permeability increased with the overall porosity except for the substrate of PES -G1.0. It was proposed by Dahe et al. [24] that uniform size distribution and nanoscale dispersion of the nanofillers in casting solution contributed to the small size nodule formation on polymer matrix, resulting in small pore size with high pore density. The NSs incorporated GO nanofillers presented higher porosity that incorporated TiO_2, which meant that GO nanoparticles exhibited better dispersion in polymer matrix. However, the PES-G1.0 substrate had the greatest overall porosity of 83.43%, but presented the lowest flux of 370 LMH among the NSs. It can be explained that the pore blocking and pore collapse due to the GO agglomeration increased to overcome the effect induced by hydrophilicity and pore size.

The digital photo images of the neat PES and NSs are exhibited in Fig. S3. Clearly, the color of the modified substrates became darker with the loading of GO. During the substrate fabrication, the movement of GO nanosheet toward top layer made a more remarkable difference in color [19]. To compare the effect of the nanofillers on the substrate morphology, the SEM images of the substrates are presented in Fig. 2. All of the substrates exhibited the typical characteristic of asymmetric porous structure for ultrafiltration membranes with a dense skin top layer and a finger-shape porous sublayer. Obviously, addition of both of the nanofillers significantly influenced the pore structure. The same observation was reported by other investigators [10,19,21]. Comparing to TiO_2, the GO nanofiller tended to form larger macrovoids as shown in cross-section of SEM. During the phase-inversion processes, the high counter diffusion velocity of solvent and non-solvent contributes to the great porosity and large pore size in membranes [25]. Due to the hydrophilic nature of the nanofillers, nanoparticles could increase the thermodynamic incompatibility between solvent and non-solvent. When the membrane formed in water, the hydrophilic nanofillers acted as barriers against direct diffusion of solvent and non-solvent which results in a faster onset of phase inversion [9]. As the more hydrophilic nature, GO nanosheets in polymer casting solution facilitate the larger macrovoids which contributed to the increase of membrane permeability and decrease of mechanical strength. The aggregated nanofiller clusters can be observed on the membrane surface for the NSs in Fig. 2. In comparison, few aggregated particles were found on the substrate of PES-T0.5/G0.5, which confirmed the speculation that the mixed nanofillers were inclined to more stable dispersion and less aggregation than the sole type nanofiller at the equal loading.

The result of examination using AFM, as shown in Fig. 3, was summarized in Table 3. The PES-T0.5/G0.5 presented the smoothest surface among the substrates. Due to the affinity toward water, the nanofillers moved toward top layer and enriched the nanoparticle concentration in the upper layer during the phase inversion [9]. It accumulates the aggregation of the nanofillers in top surface. In addition, the

Table 2
Properties of the neat and nanocomposite PES substrates

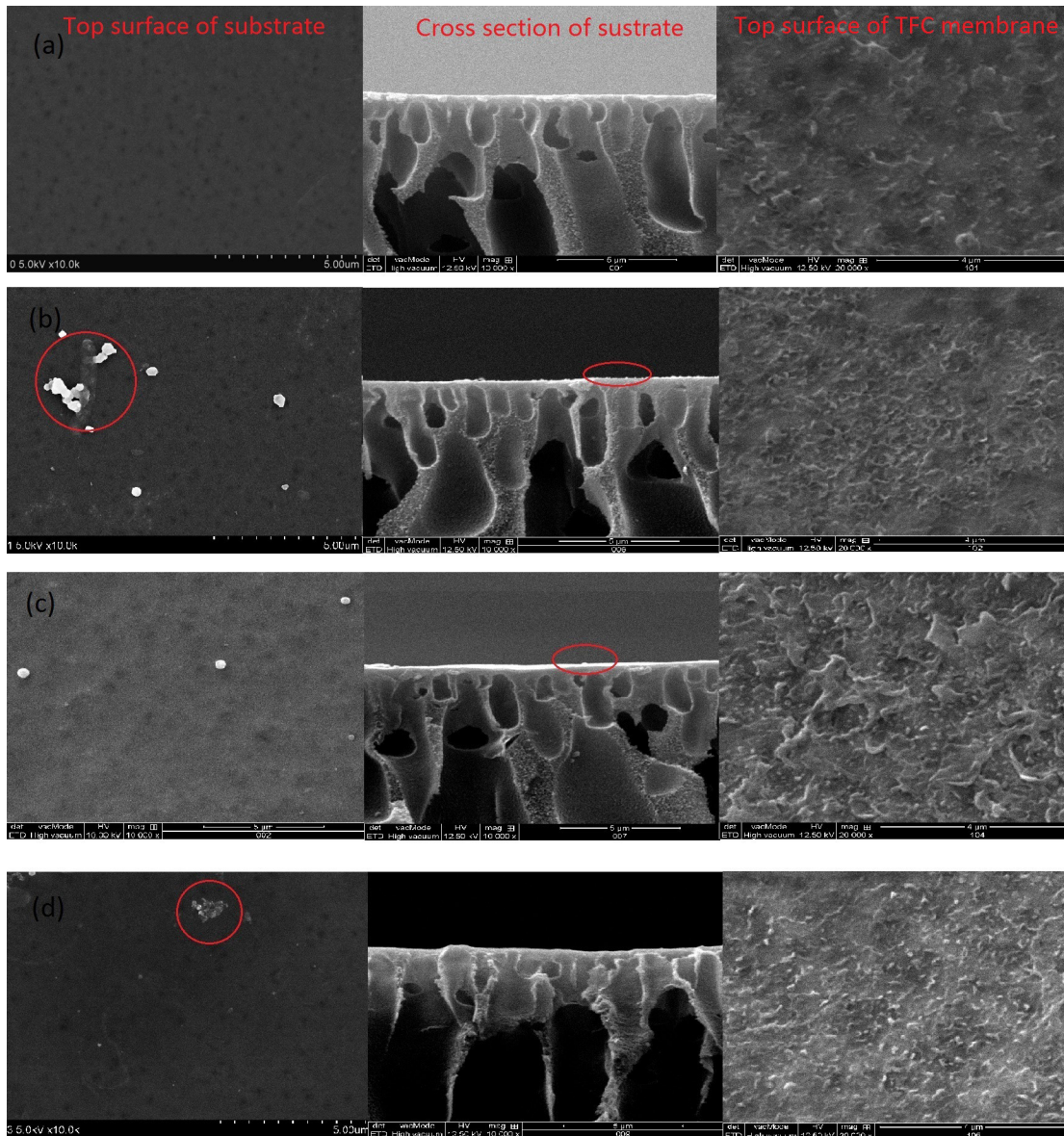| Membrane	Contact angle (°)	Overall porosity (%)	Pure water permeability (LMH bar⁻¹)
PES	95.7 ± 9.9	67.80	271 ± 22
PES-T1.0	76.9 ± 14.7	73.69	408 ± 44
PES-T0.5	73.8 ± 12.4	71.24	375 ± 36
PES-T0.5/G0.5	54.2 ± 9.6	81.05	476 ± 71
PES-G0.5	58.7 ± 8.3	81.91	452 ± 59
PES-G1.0	71.7 ± 10.8	83.43	370 ± 33

Fig. 2. Top surface and cross-section SEM images of the control (a) and modified PES substrates: PES-T1.0 (b), PES-T0.5/G0.5 (c) and PES-G1.0 (d).

Table 3
Surface roughness parameters of the substrates by AFM analysis

Membrane	R_a (nm)	R_q (nm)	R_z (nm)
PES	28.7 ± 1.0	35.7 ± 2.2	140.7 ± 23.1
PES-T1.0	12.5 ± 0.5	15.9 ± 2.2	85.1 ± 14.5
PES-T0.5	11.1 ± 1.6	15.1 ± 0.9	38.4 ± 4.1
PES-T0.5/G0.5	10.4 ± 1.3	12.1 ± 0.6	39.7 ± 10.7
PES-G0.5	10.5 ± 0.2	14.3 ± 1.5	48.2 ± 7.6
PES-G1.0	11.3 ± 1.4	15.4 ± 1.0	82.0 ± 10.1

Note: R_a is the arithmetic average of the absolute values of the surface height deviations measured from the mean plane, R_q is the root mean square average of height deviations taken from the mean data plane and R_z is maximum vertical distance between the highest and lowest data points in the image.

hydrophilic nanofillers act as barriers against the movement of non-solvent during membrane fabrication, as mentioned above. In other words, solvent molecules can diffuse more easily and rapidly from polymer structure while the polymers remained relatively stable. Thus, the smoother substrate was formed during the phase inversion.

3.2.2. Chemical composition analyses

The FTIR spectra of the substrate and TFC membrane were presented in Fig. S4. It is noted that the characteristic peaks of the symmetric stretching vibration at 1,300 cm⁻¹ and the asymmetric stretching vibration at 1,072 cm⁻¹ appear for the sulfonic acid group [26]. However, there was no discernible difference between the spectra of the neat PES and NSs incorporated with nanofillers. In the TFC spectrum,

the characteristic peaks of PA layer at 1,730 cm^{-1} which corresponds to the amide I band (C=O stretching) can be identified. The spectrum of TFC membrane appears a weak stretching at 3,400–3,600 cm^{-1} associated with the stretching vibration of the hydrogenation N–H band of TFC–FO membranes [27]. The result of energy-dispersive X-ray spectroscopy (EDX) analyses was summarized in Table 4 and Fig. S5. The presence of TiO$_2$ nanoparticles was confirmed within the substrate or on the substrate surface according to the change of element content. The content of oxygen element of the substrate increased after the addition of GO nanosheets.

Fig. 4 shows thermal gravimetric analysis (TGA) graph of the substrates and GO nanosheets. The major loss of mass for GO occurred at 150°C–200°C, which was due to CO, CO$_2$ and steam releases from the most labile functional groups. The continuous mass loss of the substrates contained GO nanosheets below 400°C is mainly ascribed to the mass loss for GO [28]. As for the TiO$_2$, the weight loss of just the TiO$_2$

powder was almost negligible. Basing on the calculation, 1% corresponded to TiO$_2$ nanofiller yields an estimate of 6.25% of residues for samples of membranes. Thus, a main mass loss from 450°C to 550°C observed for the PES substrate substrates was attributed to polymer disintegration followed by leaving a stable carbonaceous residue [29]. It was clear that TiO$_2$ addition resulted in an increase of thermal stability of the substrates. However, GO addition did not exert a significant effect on the thermal stability of the PES substrates.

Tensile tests were conducted at room temperature. The dimensions of the membrane samples were 100 mm in length and 10 mm in width. The values in Table 5 are the average of five measurements with the standard deviation quoted. It was clear that the tensile strength and Young's modulus of the substrates increased with the TiO$_2$ loading. In contrast, the tensile strength of NS incorporated with GO decreased when the loading increased from 0.5 wt% to 1 wt%. At optimum level, the nanofiller acted as a cross-linking point in composite membrane to link the polymer chain and increase the rigidity of polymer chain [30]. Consequently, more energy was needed to break down the bond between nanofiller and PES polymer chains during the tensile strength test. However, the result in Table 5 indicated that the GO addition of 1.0 wt% loading exerted insignificant effect on the mechanical property of NSs. According to the report of Park et al. [31], 1.0 wt% GO loading resulted in slightly lower tensile strength and more remarkable decrease in elongation at break in poysulfone (PSf) substrates. Ionita et al. [10] reported the similar result that raising GO loading to 0.5 and 1 wt% led to a decrease of tensile

Table 4
EDX results of the neat and nanocomposite PES substrates

Membrane	Element (wt%)				
	C	O	Na	S	Ti
PES	74.63	13.63	0	11.74	0
PES-T1	65.73	20.55	0.46	8.44	5.52
PES-T0.5/G0.5	70.23	16.15	0	11.22	1.18
PES-G1	70.88	18.40	0.61	9.38	0

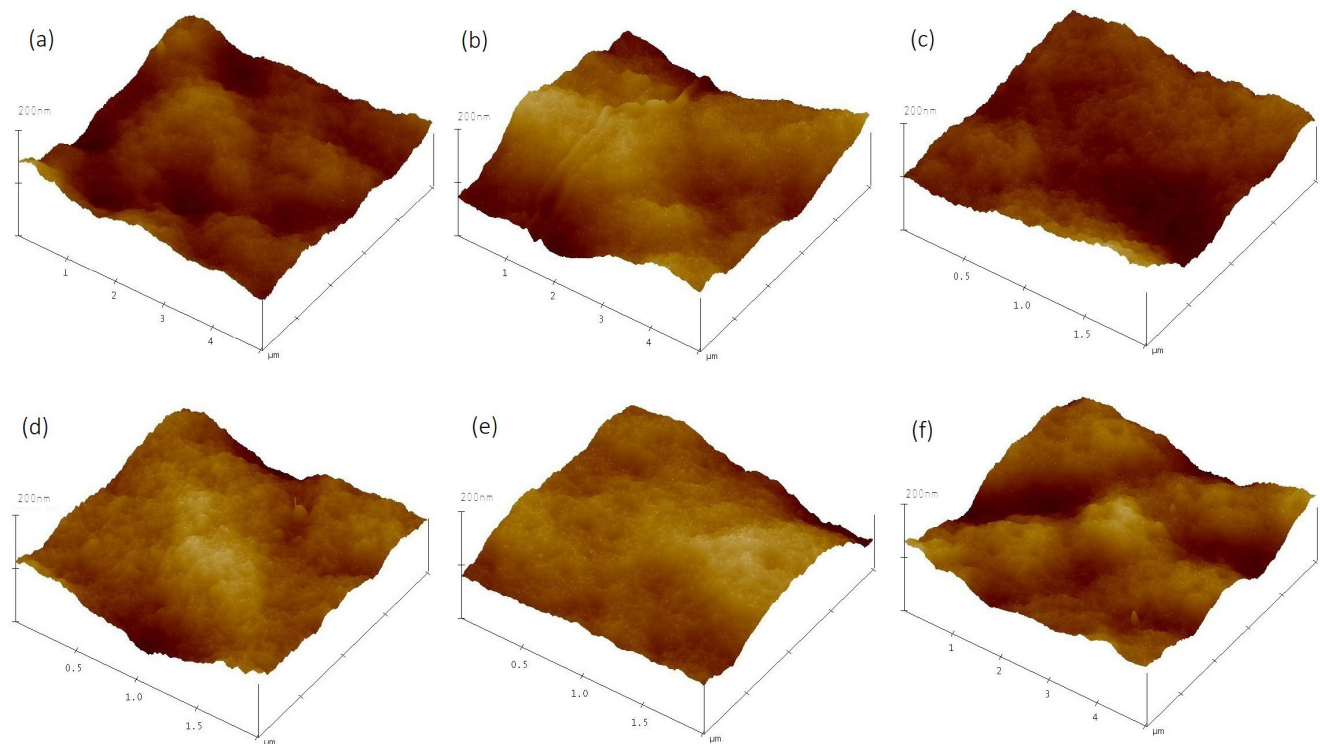

Fig. 3. AFM images of the control (a) and modified PES substrates: PES-T1.0 (b), PES-T0.5 (c), PES-T0.5/G0.5 (d), PES-G0.5 (e)and PES-G1.0 (f).
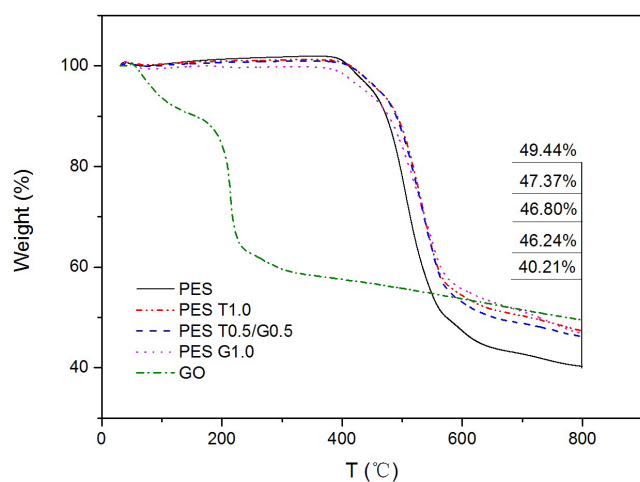
Fig. 4. TGA curve of GO and the control and modified PES substrates.

Table 5
Tensile modulus and tensile strength of nanocomposite substrates

Membrane	Young's modulus (MPa)	Tensile strength (MPa)
PES	105 ± 7	2.7 ± 0.06
PES-T1.0	151 ± 16	3.9 ± 0.08
PES-T0.5	142 ± 21	3.6 ± 0.05
PES-T0.5/G0.5	141 ± 13	3.3 ± 0.09
PES-G0.5	117 ± 10	3.3 ± 0.11
PES-G1.0	107 ± 6	2.8 ± 0.17

modulus. Nevertheless, the PSf composite membranes with 1 wt% GO loading presented about 40% of tensile strength higher than the neat sample. It was explained in the literature that the excessive presence of GO led to the aggregation and introduced more macrovoids which ultimately resulted to mechanically weaker membranes.

3.3. Characterization of the TFN membranes

3.3.1. Morphology analysis of TFN membranes

As shown in Fig. S6 (AFM images) and Table 6 (roughness parameters), the surface roughness exhibited a sharp increase after the interfacial polymerization reaction on the top surface of PES substrates. A typical "ridge-and-valley" morphology which is a typical feature of interfacial polymerized PA membranes was observed for all membranes. Apparently, all TFC-NS membranes presented smoother surface than the TFC membrane due to the rougher surface of the neat PES substrate. The membrane of TFC-NS-G1.0 fabricated at the substrate with 1 wt% GO loading had the roughest surface among the TFC-NS membranes. The reason is that the affinity of the MPD aqueous solution toward the hydrophilic nanofillers driving the MPD to diffuse slower toward the interfacial polymerization zone. As a consequence, varying thicknesses with lower peaks are formed. In addition, Lu et al. [32] proposed that the

Table 6
Surface roughness of and TFC and TFC-NS membranes by AFM analysis

Membrane	R_a (nm)	R_q (nm)	R_z (nm)
TFC	59.4 ± 8.4	84.7 ± 0.4	583.9 ± 13.4
TFC-NS-T1.0	35.8 ± 4.0	48.4 ± 4.5	341.8 ± 6.7
TFC-NS-T0.5	32.8 ± 3.8	41.4 ± 4.8	341.8 ± 65.7
TFC-NS-T0.5/G0.5	32.6 ± 8.2	44.6 ± 10.4	346.6 ± 88.7
TFC-NS-G0.5	36.9 ± 7.1	46.9 ± 5.5	348.9 ± 70.6
TFC-NS-G1.0	39.8 ± 4.1	51.0 ± 5.9	421.8 ± 103.2

Note: R_z is maximum vertical distance between the highest and lowest data points in the image, R_q is the root mean square average of height deviations taken from the mean data plane and R_a is the arithmetic average of the absolute values of the surface height deviations measured from the mean plane.

differences in transport properties and surface morphology of the TFC membranes are attributable to the different surface structures of the underlying support layers. The presence of cavities inside the ridge structure of both membranes resulted in an inhomogeneous PA film throughout its depth. Hence, more defects maybe presented in the PA film when more nanofillers were added into the support layer.

3.3.2. Intrinsic separation properties

Water flux and reverse salt leakage are the important indices to evaluate the quality of FO membranes. The water permeance and salt permeability presented in Table 7 were measured using a cross-flow RO bench-scale setup. It was obvious that the nanofiller addition in the PES substrate remarkably improved the water permeance, which was in agreement with other investigators [33]. Improvement of water permeance is likely due to three possible effects including hydrophilicity, porosity and defect. First, since the nanofillers were contiguous throughout the substrate, the hydrophilicity improvement was not limited to the membrane exterior surface but also the interior surfaces of the membrane substrate. It was conducive for water molecules to transport. Second, the substrate with high porosity generally possesses low resistance for water transportation. Third, it was inevitable that the defects caused by the nanofiller agglomeration on substrate top surface during membrane casting process. As mentioned above, nanofillers addition increased the hydrophilicity, porosity of the PES substrates. However, excessive nanofiller loading resulted in severe agglomeration which would cause more negative effects on the membrane performance. At the equal nanofiller loading, the water flux of TFC-NS-T1.0 and TFC-NS-T0.5/G0.5 were obviously lower than that of TFC-NS-G1.0 of 2.71 L/(m²·h·bar). It was speculated that severe agglomeration of GO occurred.

Along with the increase in water permeance, the salt permeability of the TFC-NS membranes also increased. The TFC membranes with neat PES substrates exhibited the highest NaCl rejection of 94.9% comparing to the TFC-NS membranes. The NaCl rejection of TFC-NS-G1.0 declined to 84.7% which was the lowest value among the TFC-NS membranes. In addition, the B/A ratio decreased as the nanofillers were

Table 7
Transport properties of TFC and TFC-NS membranes

Membrane	A		B		B/A (kPa)	R (%)	S (mm)
	LMH/bar	×10⁻¹² (m/(s Pa))	LMH	×10⁻⁸ (m/s)			
TFC	0.88	2.45	0.14	3.93	16.02	94.9	0.506
TFC-NS-T1.0	1.62	4.49	0.40	11.12	24.74	92.4	0.390
TFC-NS-T0.5	1.36	3.77	0.29	8.02	21.25	93.4	0.394
TFC-NS-T0.5/G0.5	2.25	6.24	0.47	13.04	20.90	93.5	0.396
TFC-NS-G0.5	2.04	5.65	0.69	19.14	33.86	89.9	0.424
TFC-NS-G1.0	2.71	7.53	1.47	40.87	54.26	84.7	0.275
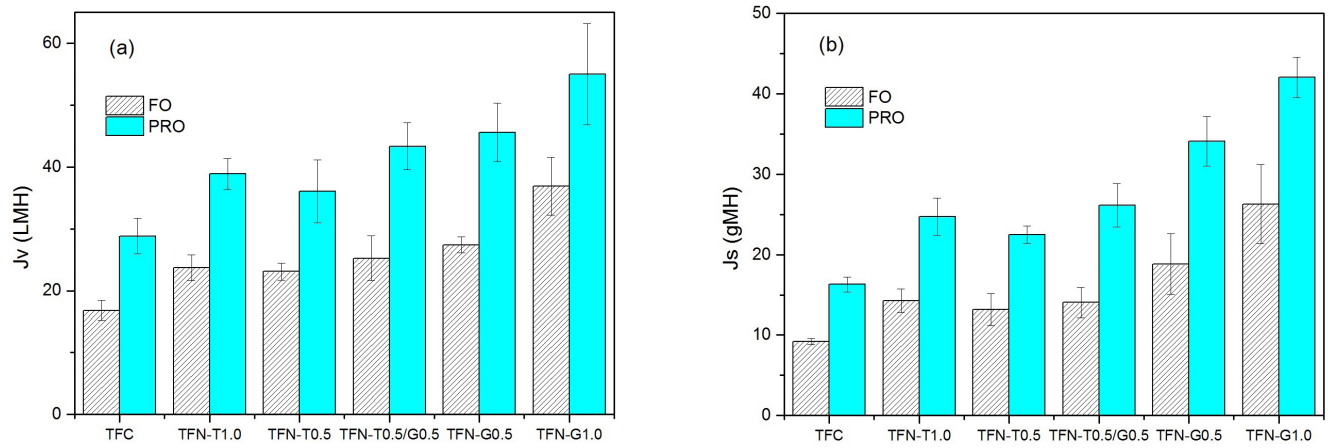
Fig. 5. (a) Water permeation flux (Jv), and (b) reverse salt flux. Crossflow velocity and temperature of both feed and draw solutions of 25 cm/s and 25°C, and DI water and 1.0 M NaCl solution were used as the feed solution and raw solution, respectively.

added into the PES matrix, and TFC-NS-T0.5/G0.5 presented the lowest *B/A* ratio of 20.9 among the TFC-NS membranes. The *B/A* is an important selectivity parameter in FO applications which is directly related to the solute reverse transport [34,35]. A lower *B/A* value is generally preferred for higher solute rejection, reduced fouling tendency and more stable operation. Recent investigation concluded the following empirical relationship [36]:

$$B = \frac{L^2}{\lambda}\left(\frac{R_g T}{M_w}\right)^3 A^3 \qquad (11)$$

where *L* is the thickness of the AL, *λ* is a fitting parameter and M_w is the solute molecular weight. This relationship provides tremendous insight for the fabrication of selective TFC membranes with low *B/A*. It can be concluded that the selectivity of PA layer was relative to the loading and property of the nanofillers. Addition of nanofillers in membrane fabrication possibly decreased the fitting parameter *λ*. The other explanation is that defects in AL may be induced by the nanomaterial clusters emerged on the substrate surface.

Fig. 5 shows the water flux (J_v) and reverse salt flux (J_s) of TFC and TFC-NS membranes in both membrane orientations with DI water and 2.0 M NaCl solution used as the FS and DS. For the TFC-NS membranes with sole type nanofiller, the water flux increased with the nanofiller loading. The phenomenon can be explained that the substrate porosity of the TFC membranes played an important role

in ICP of FO process. Therefore, less severe dilution ICP in AL-FS orientation occurred for the TFC-NS membranes with high porous substrate. However, the increasing of reverse salt flux was in consistent with the water flux. More and larger aggregated nanofiller clusters presented on the substrate surface on the TFC-NS membranes during the PA AL formation.

The structural parameter *S* value, as well as the ration of tortuosity (τ) to porosity (ε), is an important membrane substrate property that affects ICP. As single nanofiller loading in polymer matrix was proper, the addition of nanofiller is favorable to form porous microstructure which abbreviates the transport passage of solute in FO separation process and leads to a decline in the structural parameter of the membrane. The values of *S* listed in Table 7 indicated that nanomaterial incorporation in the substrate greatly improved the structure parameter and enhanced the mass transfer efficiency of the PES substrate. Compared with hand-cast TFC membranes fabricated with thin fabric support with an average *S* of 0.492 mm [37], the TFC-NS membranes exhibited lower *S* value. The TFC-NS-G1.0 exhibited the smallest *S* value of 0.275 mm. This is consistent with the substrate characterization results that PES-G1.0 had a greater porosity compared with other substrate. Obviously, the high GO loading in the substrate can optimize the structure at drawbacks of the low membrane selectivity and severe solute reverse diffusion. The first reason is the increase of membrane porosity as well as the enhancement of support layer wettability. The second

is the improvement in pore interconnectivity of support layer embedded with nanofillers. In general, synergistic effect of the mixed nanofiller on the TFC membrane for FO process was more positive than the single nanofiller.

3.4. Fouling behavior of FO membranes

The antifouling performance to BSA of TFC and TFC-NS membranes as functions of the cumulative permeate volume is shown in Fig. 6. Since AL-DS orientation was used in most FO membrane application of wastewater treatment, the antifouling test was conducted only with AL-DS orientation. It

was not surprised that the flux declined continuously during the FO experiments which was caused by membrane fouling and the decrease in osmotic driving force due to the dilution of the DS. As presented in Fig. 6, TFC-NS membranes exhibited greater resistance against organic fouling compared with the TFC membranes. GO fillers proved to be more effective to enhance the antifouling ability of the TFC-NS membranes as a modifier in the substrates than TiO_2. Although a PA AL was formed on the PES substrates after the interfacial polymerization, few nanofillers which were not all covered by PA molecules exposed to external. Consequently, the hydrophilicity of the nanoparticles mitigated the adhesion of BSA molecules
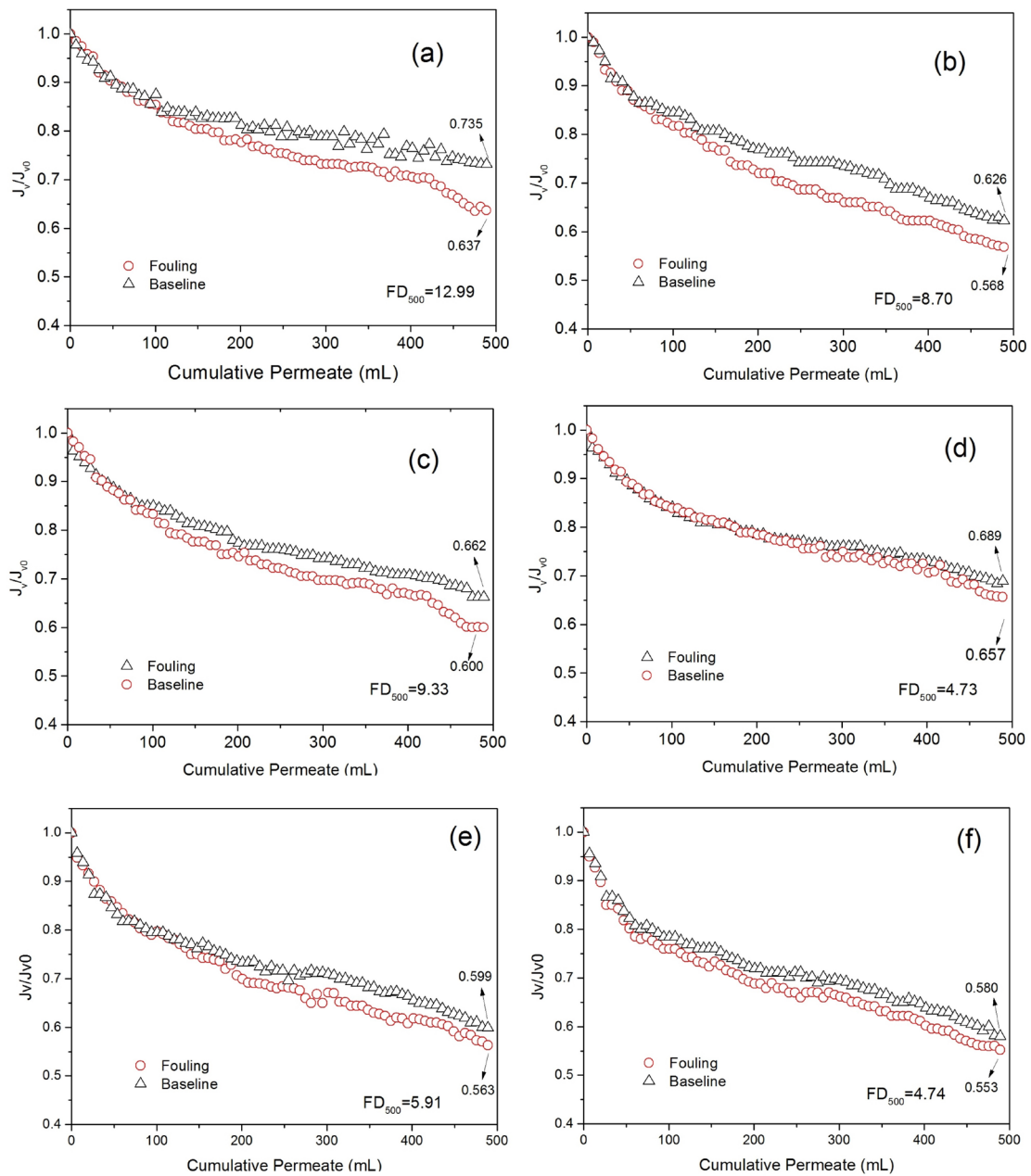

Fig. 6. The normalized flux as a function of the cumulative permeate volume of the TFC (a), TFC-NS-T1.0 (b), TFC-NS-T0.5 (c), TFC-NS-T0.5/G0.5 (d), TFC-NS-G0.5 (e) and TFC-NS-G1.0 (f) membranes during the fouling.

with hydrophobic characteristics [38]. As GO had various functional molecules of hydroxyl, carboxyl, carbonyl and epoxy groups, these inherent groups leads to a more remarkable improvement of hydrophilicity comparing to TiO_2. In addition, the GO-containing membrane surface exhibited a negative zeta potential which increased with increasing GO loading [3]. This large negative zeta potential should induce electrostatic repulsion between the membrane surface and the negatively charged carboxyl groups of BSA [40,41]. However, TFC-NS membranes suffered the severe reverse salt leakage which resulted in more flux reduction due to the nanoparticles on the membrane surface induced more defects. These defects on the PA AL caused to high leakage of reverse salt. Generally, the PES-T0.5/G0.5 possessed the best overall performance among TFC-NS membranes. It is presumed that TiO_2 and GO did not affect each other in agglomeration [42]. This is in consistent with the result of transport properties measurement of FO membranes in osmotic pressure.

4. Conclusions

In this work, TFC-NS membranes for FO process were synthesized by interfacial polymerization on the nanocomposite PES substrates which was incorporated GO and TiO_2 nanofillers. The synergistic effect of the mixed nanofillers was investigated by characterizing the NSs and TFC-NS membranes. Nanofiller addition led to increase of the hydrophilicity, water permeance, mechanical strength and thermal stability of the substrates. Similarly, transport properties of TFC-NS membranes enhanced by the nanofiller addition in PES substrates. The synergistic effect of TiO_2 and GO improving the structure of the support layer of FO membrane and enhancing the antifouling ability was more significant. In addition, the selectivity of PA AL was affected by the loading and types of the added nanofillers. The change in the water permeance and reverse salt permeability of TFC-NS membranes implied that defects on AL may be induced by the agglomerated nanofiller clusters. The antifouling property of the TFC-NS membranes was analyzed through the evaluation of flux decline in a filtration of model foulant solution. The combination of TiO_2 and GO exhibited the best overall performance among TFC-NS membranes.

Acknowledgment

References

[1] M. Elimelech, W.A. Phillip, The future of seawater desalination: energy, technology, and the environment, Science, 333 (2011) 712–717.

[2] B. Van der Bruggen, P. Luis, Forward osmosis: understanding the hype, Rev. Chem. Eng., 31 (2015) 1–12.

[3] H.Y. Jin, Y.B. Huang, X. Wang, P. Yu, Y.B. Luo, Preparation of modified cellulose acetate membranes using functionalized multi-walled carbon nanotubes for forward osmosis, Desal. Wat. Treat., 57 (2016) 7166–7174.

[4] M. Amini, A. Rahimpour, M. Jahanshahi, Forward osmosis application of modified TiO_2-polyamide thin film nanocomposite membranes, Desal. Wat. Treat., 57 (2016) 14013–14023.

[5] S.G. Kim, D.H. Hyeon, J.H. Chun, B.H. Chun, S.H. Kim, Novel thin nanocomposite RO membranes for chlorine resistance, Desal. Wat. Treat., 51 (2013) 6338–6345.

[6] L. Shen, S. Xiong, Y. Wang, Graphene oxide incorporated thin-film composite membranes for forward osmosis applications, Chem. Eng. Sci., 143 (2016) 194–205.

[7] F.S. Kamelian, S.M. Mousavi, A. Ahmadpour, Al_2O_3 and TiO_2 entrapped ABS membranes: preparation, characterization and study of irradiation effect, Appl. Surf. Sci., 357 (2015) 1481–1489.

[8] X. Chang, Z. Wang, S. Quan, Y. Xu, Z. Jiang, L. Shao, Exploring the synergetic effects of graphene oxide (GO) and polyvinylpyrrodione (PVP) on poly(vinylylidenefluoride) (PVDF) ultrafiltration membrane performance, Appl. Surf. Sci., 316 (2014) 537–548.

[9] Y. Wang, R. Ou, H. Wang, T. Xu, Graphene oxide modified graphitic carbon nitride as a modifier for thin film forward osmosis membrane, J. Membr. Sci., 475 (2015) 281–289.

[10] M. Ionita, E. Vasile, L.E. Crica, S.I. Voicu, A.M. Pandele, S. Dinescu, L. Predoiu, B. Galateanu, A. Hermenean, M. Costache, Synthesis, characterization and in vitro studies of polysulfone/graphene oxide composite membranes, Composites Part B, 72 (2015) 108–115.

[11] D.C. Marcano, D.V. Kosynkin, J.M. Berlin, A. Sinitskii, Z. Sun, A. Slesarev, L.B. Alemany, W. Lu, J.M. Tour, Improved synthesis of graphene oxide, ACS Nano, 4 (2010) 4806–4814.

[12] N. Widjojo, T.-S. Chung, M. Weber, C. Maletzko, V. Warzelhan, A sulfonated polyphenylenesulfone (sPPSU) as the supporting substrate in thin film composite (TFC) membranes with enhanced performance for forward osmosis (FO), Chem. Eng. J., 220 (2013) 15–23.

[13] T.Y. Cath, M. Elimelech, J.R. McCutcheon, R.L. McGinnis, A. Achilli, D. Anastasio, A.R. Brady, A.E. Childress, I.V. Farr, N.T. Hancock, J. Lampi, L.D. Nghiem, M. Xie, N.Y. Yip, Standard methodology for evaluating membrane performance in osmotically driven membrane processes, Desalination, 312 (2013) 31–38.

[14] S.R.-V. Castrillon, X. Lu, D.L. Shaffer, M. Elimelech, Amine enrichment and poly(ethylene glycol) (PEG) surface modification of thin-film composite forward osmosis membranes for organic fouling control, J. Membr. Sci., 450 (2014) 331–339.

[15] M. Park, J.J. Lee, S. Lee, J.H. Kim, Determination of a constant membrane structure parameter in forward osmosis processes, J. Membr. Sci., 375 (2011) 241–248.

[16] J. Zhang, Z. Xu, W. Mai, C. Min, B. Zhou, M. Shan, Y. Li, C. Yang, Z. Wang, X. Qian, Improved hydrophilicity, permeability, antifouling and mechanical performance of PVDF composite ultrafiltration membranes tailored by oxidized low-dimensional carbon nanomaterials, J. Mater. Chem. A, 1 (2013) 3101–3111.

[17] X. Fan, W. Peng, Y. Li, X. Li, S. Wang, G. Zhang, F. Zhang, Deoxygenation of exfoliated graphite oxide under alkaline conditions: a green route to graphene preparation, Adv. Mater., 20 (2008) 4490–4493.

[18] G.X. Zhao, J.X. Li, X.M. Ren, C.L. Chen, X.K. Wang, Few-layered graphene oxide nanosheets as superior sorbents for heavy metal ion pollution management, Environ. Sci. Technol., 45 (2011) 10454–10462.

[19] B. Ganesh, A.M. Isloor, A. Ismail, Enhanced hydrophilicity and salt rejection study of graphene oxide-polysulfone mixed matrix membrane, Desalination, 313 (2013) 199–207.

[20] L. Hamming, X. Fan, P. Messersmith, L. Brinson, Mimicking mussel adhesion to improve interfacial properties in composites, Compos. Sci. Technol., 68 (2008) 2042–2048.

[21] A. Razmjou, J. Mansouri, V. Chen, The effects of mechanical and chemical modification of TiO_2 nanoparticles on the surface chemistry, structure and fouling performance of PES ultrafiltration membranes, J. Membr. Sci., 378 (2011) 73–84.

[22] H. Wang, X. Yuan, Y. Wu, H. Huang, X. Peng, G. Zeng, H. Zhong, J. Liang, M.M. Ren, Graphene-based materials: fabrication, characterization and application for the decontamination of wastewater and wastegas and hydrogen storage/generation, Adv. Colloid Interface Sci., 195–196 (2013) 19–40.

[23] S. Zhao, P. Wang, C. Wang, X. Sun, L. Zhang, Thermostable PPESK/TiO$_2$ nanocomposite ultrafiltration membrane for high temperature condensed water treatment, Desalination, 299 (2012) 35–43.

[24] G.J. Dahe, R.S. Teotia, J.R. Bellare, The role of zeolite nanoparticles additive on morphology, mechanical properties and performance of polysulfone hollow fiber membranes, Chem. Eng. J., 197 (2012) 398–406.

[25] W.F.C. Kools, Membrane Formation by Phase Inversion in Multicomponent Polymer Systems, Mechanisms and Morphologies, PhD Thesis, University of Twente, 1998.

[26] Q. Jia, Y. Xu, J. Shen, H. Yang, L. Zhou, Effects of hydrophilic solvent and oxidation resistance post surface treatment on molecular structure and forward osmosis performance of polyamide thin-film composite (TFC) membranes, Appl. Surf. Sci., 356 (2015) 1105–1116.

[27] K.Y. Wang, T.S. Chung, G. Amy, Developing thin-film-composite forward osmosis membranes on the PES/SPSf substrate through interfacial polymerization, AIChE J., 58 (2012) 770–781.

[28] A. Sotto, A. Boromand, R. Zhang, P. Luis, J.M. Arsuaga, J. Kim, B. Van der Bruggen, Effect of nanoparticle aggregation at low concentrations of TiO$_2$ on the hydrophilicity, morphology, and fouling resistance of PES–TiO$_2$ membranes, J. Colloid Interface Sci., 363 (2011) 540–550.

[29] T. Forati, M. Atai, A. Rashidi, M. Imani, A. Behnamghader, Physical and mechanical properties of graphene oxide/polyethersulfone nanocomposites, Polym. Adv. Technol., 25 (2014) 322–328.

[30] J.-F. Li, Z.-L. Xu, H. Yang, L.-Y. Yu, M. Liu, Effect of TiO$_2$ nanoparticles on the surface morphology and performance of microporous PES membrane, Appl. Surf. Sci., 255 (2009) 4725–4732.

[31] M.J. Park, S. Phuntsho, T. He, G.M. Nisola, L.D. Tijing, X.-M. Li, G. Chen, W.-J. Chung, H.K. Shon, Graphene oxide incorporated polysulfone substrate for the fabrication of flat-sheet thin-film composite forward osmosis membranes, J. Membr. Sci., 493 (2015) 496–507.

[32] X. Lu, S. Nejati, Y. Choo, C.O. Osuji, J. Ma, M. Elimelech, Elements provide a clue: nanoscale characterization of thin-film composite polyamide membranes, ACS Appl. Mater. Interfaces, 7 (2015) 16917–16922.

[33] M. Ghanbari, D. Emadzadeh, W.J. Lau, H. Riazi, D. Almasi, A.F. Ismail, Minimizing structural parameter of thin film composite forward osmosis membranes using polysulfone/halloysite nanotubes as membrane substrates, Desalination, 377 (2016) 152–162.

[34] W.C.L. Lay, J. Zhang, C. Tang, R. Wang, Y. Liu, A.G. Fane, Analysis of salt accumulation in a forward osmosis system, Sep. Sci. Technol., 47 (2012) 1837–1848.

[35] D.L. Shaffer, J.R. Werber, H. Jaramillo, S. Lin, M. Elimelech, Forward osmosis: where are we now?, Desalination, 356 (2015) 271–284.

[36] G.M. Geise, H.B. Park, A.C. Sagle, B.D. Freeman, J.E. McGrath, Water permeability and water/salt selectivity tradeoff in polymers for desalination, J. Membr. Sci., 369 (2011) 130–138.

[37] N.Y. Yip, A. Tiraferri, W.A. Phillip, J.D. Schiffman, M. Elimelech, High performance thin-film composite forward osmosis membrane, Environ. Sci. Technol., 44 (2010) 3812–3818.

[38] D. Emadzadeh, W. Lau, T. Matsuura, N. Hilal, A. Ismail, The potential of thin film nanocomposite membrane in reducing organic fouling in forward osmosis process, Desalination, 348 (2014) 82–88.

[39] B. Yu, B. Zhao-Yong, Z. Jun-Xiao, D. Ai-Zhong, L. Shao-Lei, W. Hui, Effect of the oxygen-containing functional group of graphene oxide on the aqueous cadmium ions removal, Appl. Surf. Sci., 329 (2015) 269–275.

[40] S.A. Kiran, Y.L. Thuyavan, G. Arthanareeswaran, T. Matsuura, A.F. Ismail, Impact of graphene oxide embedded polyethersulfone membranes for the effective treatment of distillery effluent, Chem. Eng. J., 286 (2016) 528–537.

[41] P. Zhao, B.Y. Gao, Q.Y. Yue, H.K. Shon, Q. Li, Fouling of forward osmosis membrane by protein (BSA): effects of pH, calcium, ionic strength, initial permeate flux, membrane orientation and foulant composition, Desal. Wat. Treat., 57 (2016) 13415–13424.

[42] Q. Zhang, Y. He, X. Chen, D. Hu, L. Li, T. Yin, L. Ji, Structure and photocatalytic properties of TiO$_2$-graphene oxide intercalated composite, Chin. Sci. Bull., 56 (2011) 331–339.
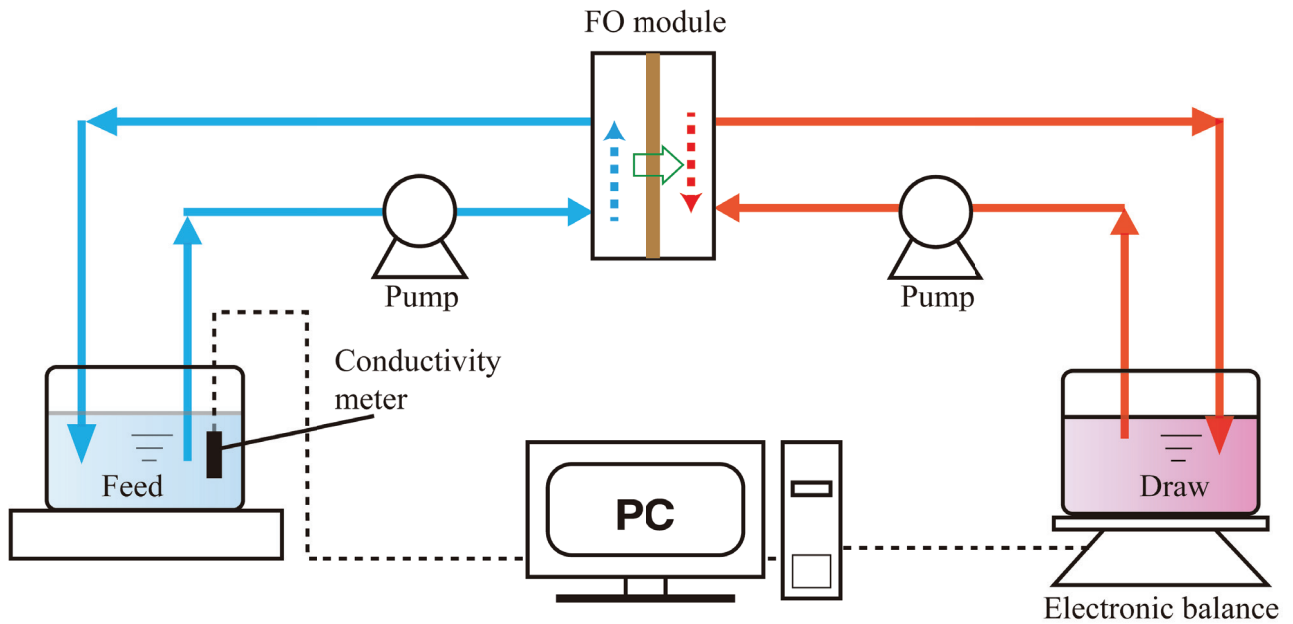
Supplementary information

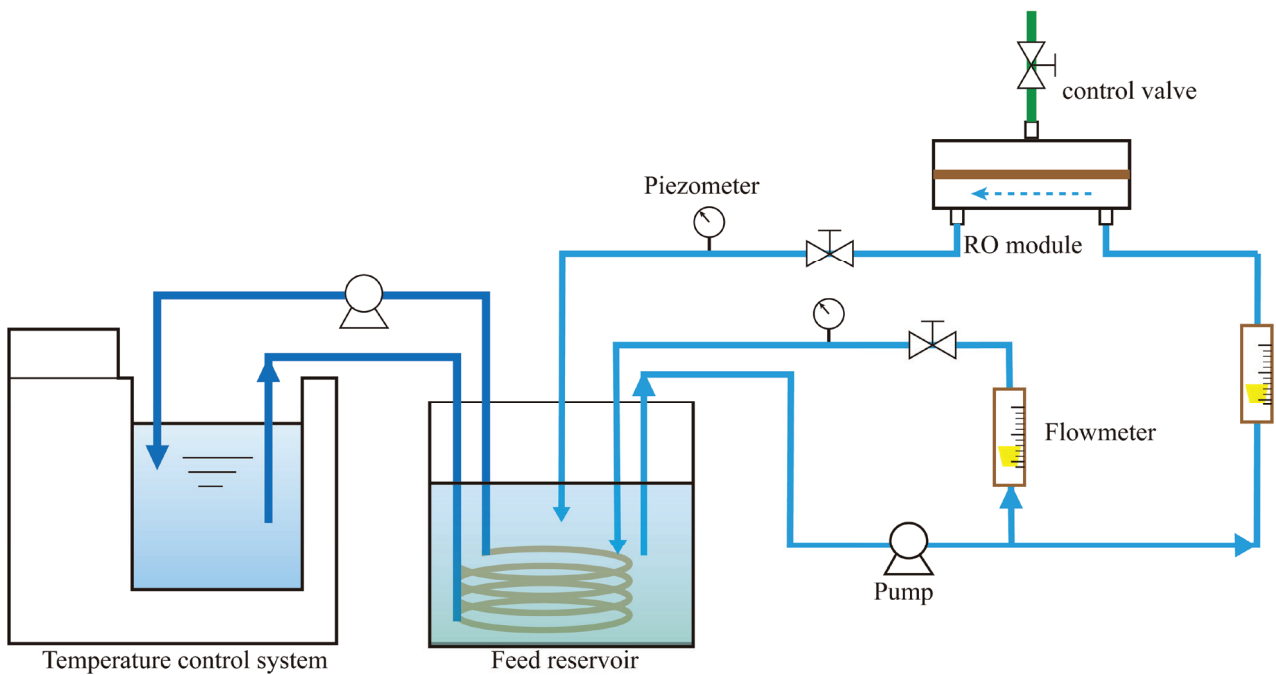Fig. S1. Cross-flow reverse osmosis setup for membrane separation performance tests.

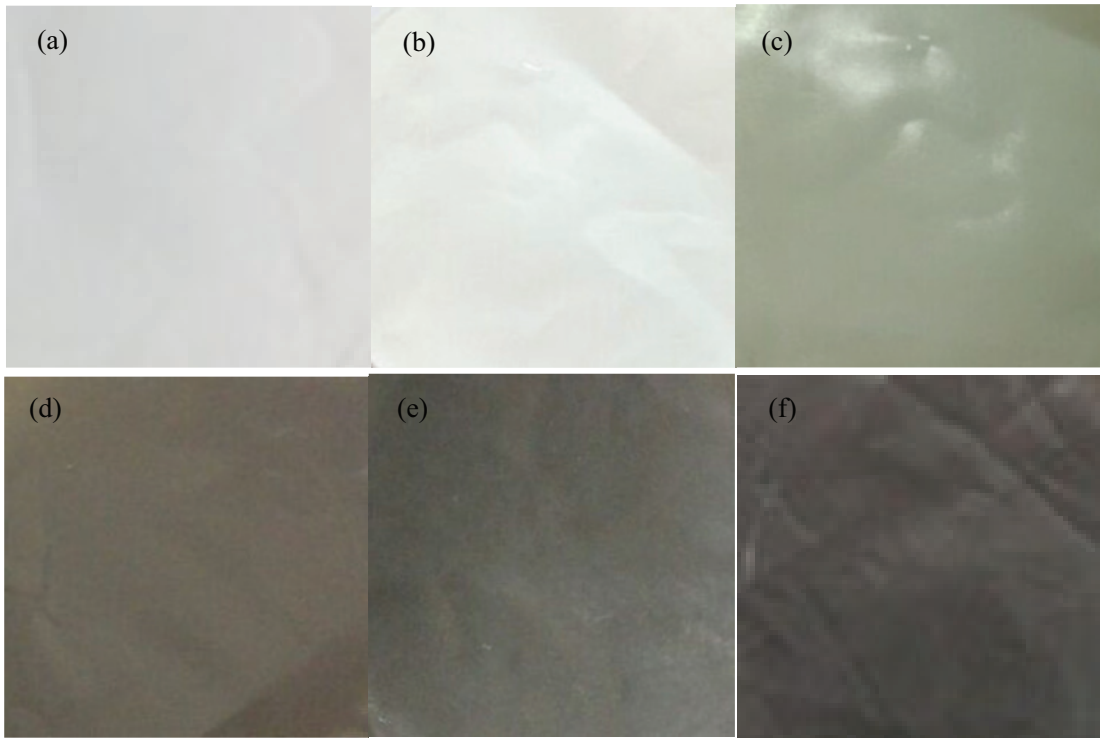Fig. S2. Schematic diagram of the laboratory-scale forward osmosis (FO) system.

Fig. S3. Photographs of the control (a) and modified PES substrates: PES-T1.0 (b), PES-T0.8/G0.2 (c), PES-T0.5/G0.5 (d), PES-T0.2/G0.8 (e) and PES-G1.0 (f).
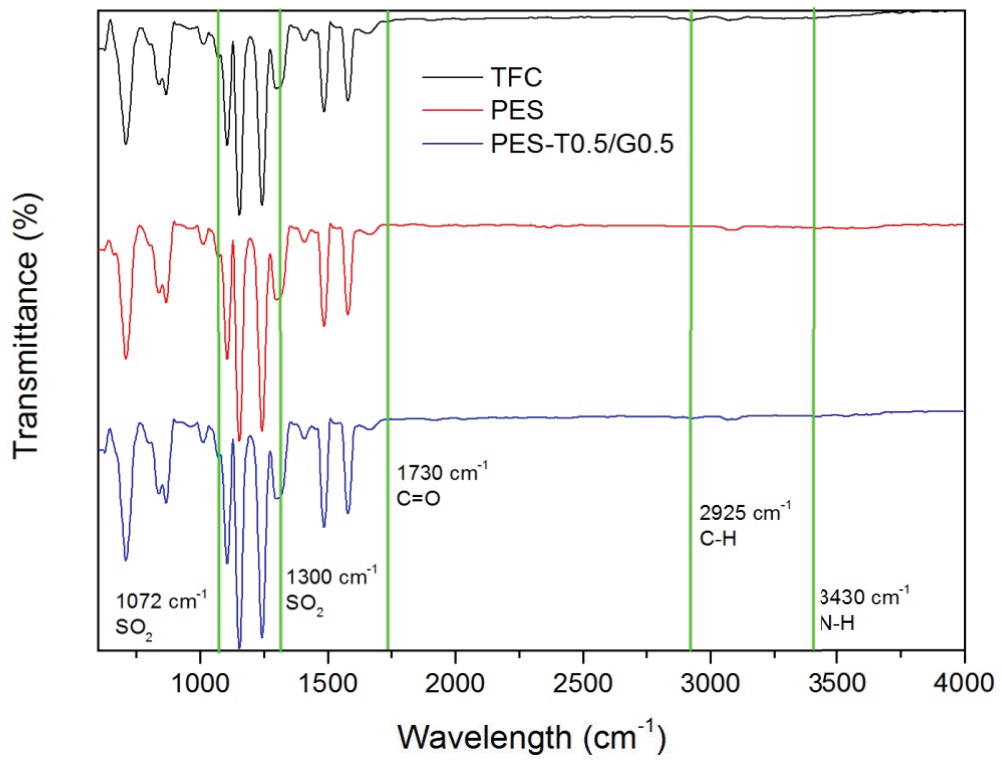

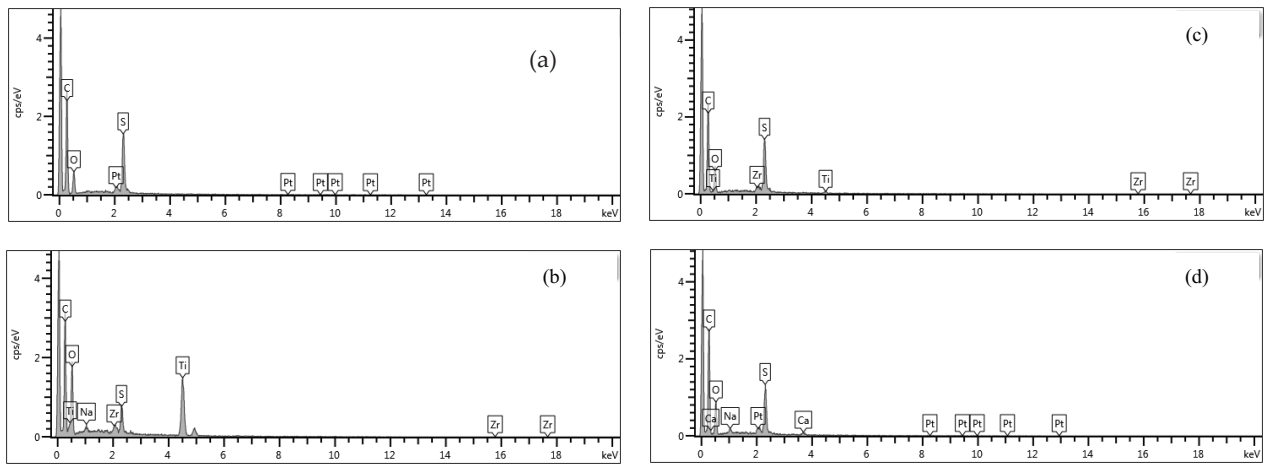Fig. S4. ATR-FTIR spectra of the PES substrates and TFC membrane.

Fig. S5. EDX patterns of the top surface of the control (a) and modified PES substrates, the control (a) and substrates of PES-T1.0 (b), PES-T0.5/G0.5 (c) and PES-G1.0 (d).
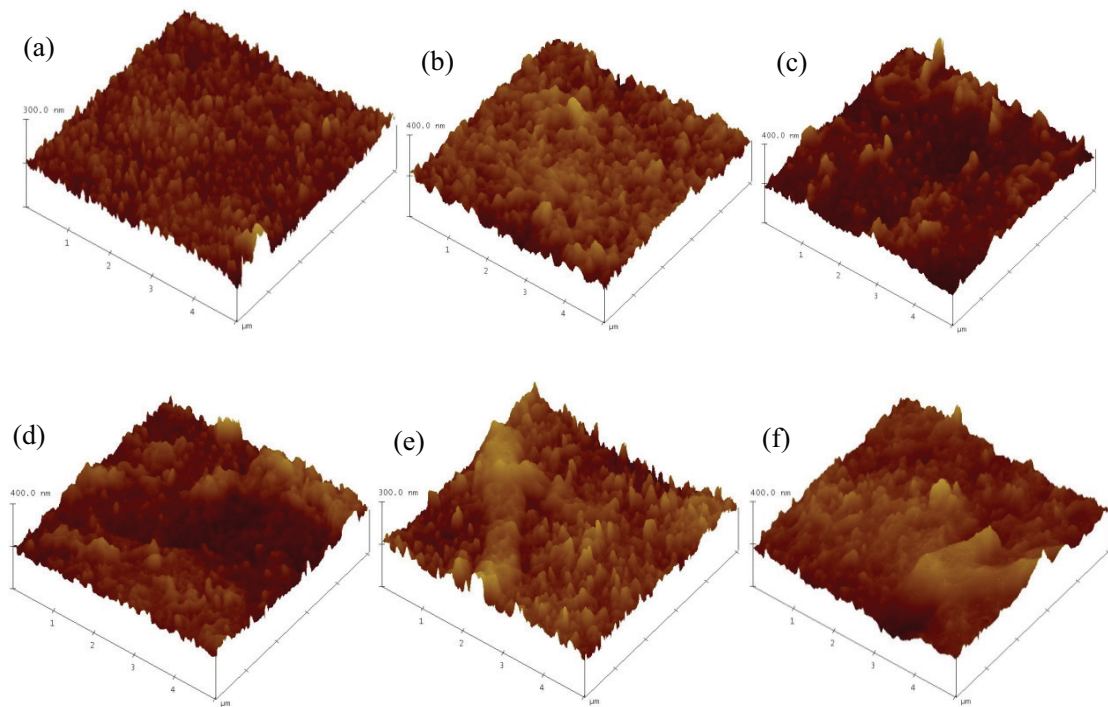

Fig. S6. AFM images of the control TFC (a) and TFC-NS membranes: TFC-NS-T1.0 (b), TFC-NS-T0.8/G0.2 (c), TFC-NS-T0.5/G0.5 (d), TFC-NS-T0.2/G0.8 (e), and TFC-NS-G1.0 (f).